Mechanical properties of rolled A356 based composites reinforced by Cu-coated bimodal ceramic particles

N. Beigi Khosroshahi [a], R. Taherzadeh Mousavian [a,⇑], R. Azari Khosroshahi [a], D. Brabazon [b]

[a] *Faculty of Materials Engineering, Sahand University of Technology, Tabriz, Iran*
[b] *Advanced Processing Technology Research Centre, School of Mechanical & Manufacturing Engineering, Dublin City University, Dublin 9, Ireland*

abstract

Three kinds of A356 based composites reinforced with 3 wt.% Al_2O_3 (average particle size: 170 lm), 3 wt.% SiC (average particle size: 15 lm), and 3 wt.% of mixed Al_2O_3–SiC powders (a novel composite with equal weights of reinforcement) were fabricated in this study via a two-step approach. This first process step was semi-solid stir casting, which was followed by rolling as the second process step. Electroless deposition of a copper coating onto the reinforcement was used to improve the wettability of the ceramic particles by the molten A356 alloy. From microstructural characterization, it was found that coarse alumina particles were most effective as obstacles for grain growth during solidification. The rolling process broke the otherwise present fine silicon platelets, which were mostly present around the Al_2O_3 particles. The rolling process was also found to cause fracture of silicon particles, improve the distribution of fine SiC particles, and eliminate porosity remaining after the first casting process step. Examination of the mechanical properties of the obtained composites revealed that samples which contained a bimodal ceramic reinforecment of fine SiC and coarse Al_2O_3 particles had the highest

Keywords:
A356, Metal matrix composite Bimodal, Ceramics Rolling, Mechanical properties, strength and hardness.

1. Introduction

The use of Al–Si (in particular A356) alloys in the manufacture of automotive engine components has considerably increased. The main benefits from usage of these alloys is their ease of manufacturability, high wear resistance, low thermal expansion coefficient, good corrosion resistance, low density and improved elevated temperature properties [1,2]. Although high-strength aluminum alloys have been developed, the addition of alloying elements and microstructural modification, can be costly, contain toxic elements, and often results in properties, which only result in a slight increase in stiffness. The demands for lightweight, high-modulus, and high-strength materials have therefore led to the development of aluminum metal matrix composites (AMMCs) [3–8].

Stir casting in the semi-solid state is the most frequently used method for production of particulate AMMCs [9–19]. Coating or oxidizing the reinforcement particles, adding some surface-active elements such as magnesium into the matrix, and stirring of metal matrix alloy for an adequate time period during incorporation are some ways used in the semi-solid stir casting process to aid particle incorporation and chemical bonding with the matrix [5,7,13,20–26]. Coating of the reinforcement is a successful technique used to promote wetting of the particles by aluminum through decreasing the surface energy of the solid–liquid (c_{sl}). In 1981, Rohatgi [27] suggested the usage of copper electroless coating on mica particles for increasing their wettability by molten aluminum. In 1998, Rajan and co-workers studied on the role of particulate reinforcement coating on the wettability and interface characteristics of aluminum metal matrix composites [22]. They reported that the copper coating dissolves into the aluminum matrix to form a solid solution, simultaneously exposing the surface to the melt directly and thereby improving the wettability of ceramic by the aluminum matrix. They have shown the formation of $CuAl_2$ phase, with an endothermic nature, at the interface of matrix/reinforcement. In 2006, Leon and co-workers studied the wettability and spreading kinetics of molten aluminum on copper-coated ceramics using a sessile drop technique [28]. They have shown that after 2 min exposure of copper-coated ceramics by aluminum melt drop that the contact angle decreased to 12.6 and 26 for Al/Cu–Al_2O_3 and Al/Cu–SiC, respectively.

Several mechanical processes including compressing, rolling, extrusion, forging, equal channel angular pressing (ECAP) and accumulative roll bonding (ARB) have been applied to as-cast AMMCs and it has been shown that they can improve the mechanical properties of the AMMCs. The observed improvement in ductility and strength is attributed to associated (a) decrease in porosity content, (b) better interfacial bonding between particle and matrix, (c) separation of agglomerated particles, and (d) refinement of the matrix structure [5,29–37].

Recently, the researchers [38–45] have been focused on fabrication of a composite materials, which contain ceramic reinforcement particles with bimodal or trimodal particle size distributions. It has been reported in literature [44,45] that the usage of lower ceramic particle size would lead to a better hardness, yield strength, tensile strength, and wear resistance. As an explanation for this, it is noted as that finer particles provide a higher number of barriers per unit volume compared with composites reinforced with a larger particle size at the same weight percentage. However, it has also been found that decreasing the particle size leads to a higher occurrence of particle agglomeration and a poor particle distribution would be obtained [44,45]. On the other hand, some of the researchers [41,45] suggested that the usage of larger ceramic particles improves some mechanical or physical properties and the use of such particles is preferred in specific applications. Deng et al. [46] fabricated bimodal size particle reinforced AZ91 magnesium matrix composites via the stir casting process. They have found that larger particles were more able to produce grain refinement than smaller ones and that the yield strength of the bimodal size SiC/AZ91 composite was higher than that of the single-sized particle reinforced composites. Cerit [47] investigated the low-speed impact behavior of dual particle size aluminum matrix composites reinforced with SiC particles, fabricated via a powder metallurgy route. It was reported from this work that while the dual particle size composite may have improved hardness and impact performance compared to single particle size

composite, agglomeration of the finer reinforcement may also have had a negative affect on the hardness and impact behavior. Large particles proved useful in this regard to prevent such agglomerations in the dual particle sized composites. Shen et al. [45] studied the effect of bimodal distribution of SiC particulates on the microstructure and mechanical properties of AZ31B magnesium matrix composites. They have reported that larger-sized SiC particle played a significant role on the reduction of thermal expansion coefficients (CTEs), and the average grain size of the composites reinforced with larger-sized SiC particles was lower than that of the smaller-sized SiC particles reinforced composites. They also reported that both the ultimate tensile strength and yield strength of the AZ91D magnesium alloy increased with the increase of smaller-sized submicron SiC content, while the agglomeration would appear in the composite if the smaller sized SiC content exceeds 2 vol.%. They have concluded that compared with the monolithic AZ31B matrix alloy and a single particle size distribution of SiC reinforced magnesium matrix composites, the ultimate tensile strength and yield strength of bimodal size SiC reinforced magnesium matrix composite were enhanced.

To the best of our knowledge, no attempt has been made to study the effect of bimodal micron sized ceramic particles on the microstructure, tensile behavior, and hardness of A356 aluminum matrix composite, fabricated through semi-solid stir casting followed by the rolling process. In this study, A356 based composites were fabricated via two-step casting process which consisted of semi-solid casting followed by rolling. Coarse Al_2O_3 and fine SiC particles were separately used as reinforcement for two of the samples; and a novel sample with equal weight mixture of these powders was prepared in order to explore the effect of using a bimodal ceramic particle size distribution on the mechanical properties.

2. Experimental procedure

A356 aluminum ingot was used as a matrix. Table 1 tabulates the chemical composition of the ingot used in this work as obtained using a M5000 optical emission spectrometer, Focused Photonics Inc., China.

Table 1
Chemical composition (in wt.%) of A356 aluminum alloy used in this study.

Al%	Si%	Mg%	Fe%	Cu%	Mn%	Zn%	Ni%	Ti%
Bal.	7.2	0.33	0.11	0.01	0.02	0.02	0.03	0.01

Micron-sized SiC particles with an average particle size of 15 lm and 99.7% purity as well as coarse alumina particles with an average particle size of 170 lm and 99.4% purity were supplied from Shanghai Dinghan Chemical Co., Ltd. China, as the reinforcement. The morphology of these ceramic particles is shown in Fig. 1. The preparation procedure used for production of the copper coating on the SiC particles via ED was reported in our previous study [20]. Table 2 shows the chemicals, their concentrations, and other process parameters (pH, temperature, and stirring speed) which were used.

Table 2
Composition of bath and coating parameters used for electroless deposition of the copper coating onto the ceramic particles.

Role in bath	Composition		Concentration
Main salt	Copper sulfate	$CuSO_4{\cdot}5H_2O$	18 g/l
Reducing agent	Formaldehyde	HCHO	20 g/l
Complexing agent	Potassium sodium tartrate	$C_4H_4O_6KNa{\cdot}4H_2O$	48 g/l
pH adjuster	Sodium hydroxide	NaOH	To adjust pH
Ceramic powders (SiC/Al_2O_3)			22.5 g/ 1000 ml
Operation	Magnetic stirring		400 rpm
	Temperature		60 °C
	pH		10

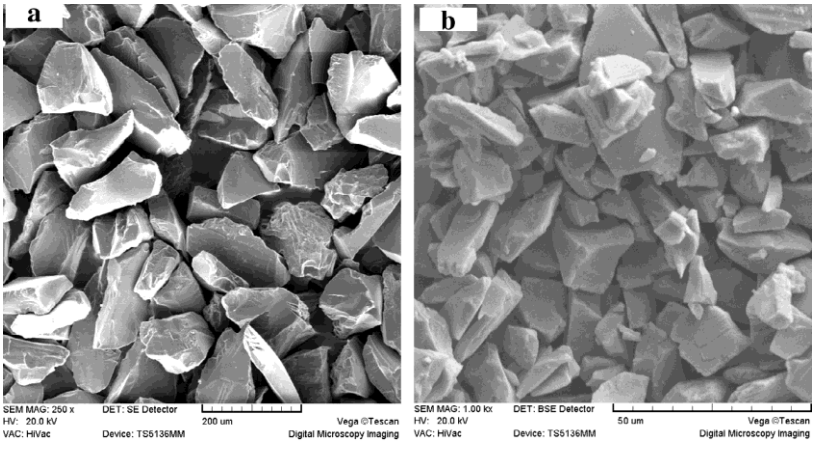

Fig. 1. SEM morphology of (a) 170 lm average particle size Al_2O_3 powders, and (b) 15 lm average particle size SiC powders.

Four sample types were fabricated in this study for comparison of the effects ceramic addition to the matrix, ceramic type, and bimodal size ceramic particles on the microstructure and mechanical properties of the composites. Table 3 summaries the characteristics of the four sample types prepared in this study and the weight of the ceramic powders before and after ED.

One gram of reinforcement powder for the composite samples was encapsulated carefully in an aluminum foil packet before the stir casting process in order to fabricate a composite with 3 wt.% ceramic powders as reinforcement. The coated powders were wrapped by hand in aluminum foil with a precaution taken not to abrade the coated ceramics. These packets were pre-heated at 350 C for 2 h in order to remove the moisture and impurities from the powders. The A356 alloy (500 g) was heated to 640 C using a resistance furnace in order to have uniform melt condition. The melt was cooled to 600 C corresponding to a 0.3 solid fraction, based on analysis with Thermo-calc software (see Fig. 2) and pervious literature [11].

Table 3
Characteristics of the samples fabricated in this study and weight of the powders after (and before) the ED process.

Samples	Characteristics	Powder weight
S_1	A356 as matrix	–
S_2	A356 as matrix, 3 wt.% alumina as reinforcement	17.60 (15 g alumina + 2.6 g Cu)
S_3	A356 as matrix, 3 wt.% SiC as reinforcement	18.43 (15 g SiC + 3.43 g Cu)
S_4	A356 as matrix, 1.5 wt.% alumina and 1.5 wt.% SiC as reinforcement	18.05 (7.5 g alumina + 7.5 g SiC + 3.05 g Cu)

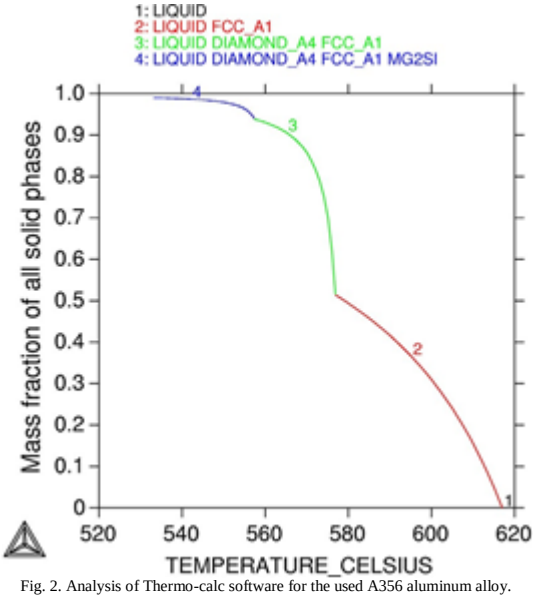

Fig. 2. Analysis of Thermo-calc software for the used A356 aluminum alloy.

A ZrO_2 coated-stainless steel stirrer was placed below the surface of melt, rotated with a speed of 500 rpm, while high purity argon gas was simultaneously applied as a protective shroud on the melt surface. During the stir-casting process, the aluminum foil packets were added to the vortex center at 600 C during the first minute of the semi-solid stirring. The temperature of the melt was then increased just after packets addition to 630 C, above the melting point of A356 alloy, and the stirring was continued for another 5 min. An addition of 1 wt.% Mg was also added during the ceramic addition feeding process, to improve their wettability by molten metal. The composite slurry in liquid state was poured into a low-carbon steel mold (at 25 C). A schematic of the stir-casting set-up and its bottom-pouring system was shown in detail in Fig. 3. This figure also shows the central location from which the samples were taken from the composite casting for rolling and subsequent characterization.

Samples of 70 mm length, 15 mm width, and 6 mm thickness were machined from solidified composites before rolling. The machined composite samples were held for 30 min at 500 C in a preheated furnace and then were hot-rolled with four passes and with a thickness reduction of 1 mm per pass (67% reduction) and followed by one cold rolling pass at room temperature with a thickness reduction of 20%, resulting in a final sheet thickness of 1.6 mm. The rolling process was carried out with no lubrication, using a laboratory rolling mill with a loading capacity of 30 tons. The roll diameter was 350 mm and the rolling speed was set at 10 rpm. The tensile tests were performed at room temperature using an Universal tensile testing machine operating at a constant rate of crosshead displacement, with an initial set strain rate of 2 10 ^{3} s ^{1}. The YS, UTS, and ductility (% elongation to break) were measured and averaged over 3 test samples. The plate tensile specimens had a gauge length of 8.3 mm and were prepared in accordance with ASTM E8M standard. Fig. 4 shows a schematic of rolling process with four hot and one cold roll pass, as well as the dimensions of tensile test samples.

Microhardness testing was conducted according to ASTM E384 using an applied load of 50 g for a 15 s duration. At least ten measurements were taken from the rolled samples. A scanning electron microscope (SEM, Cam Scan MV2300, equipped with

EDAX analysis), an optical microscopy (OM, Olympus equipped with digital camera model DP73), and image analyzer software (ClemexVision 3.5) were used for microstructural investigations. For this purpose, the samples were ground, polished, and etched with Keller's reagent (190 ml water, 5 ml HNO_3, 3mlHCl, and 2 ml HF). The average porosity contents of the produced samples in as-cast and rolled conditions were determined using the Archimedean method.

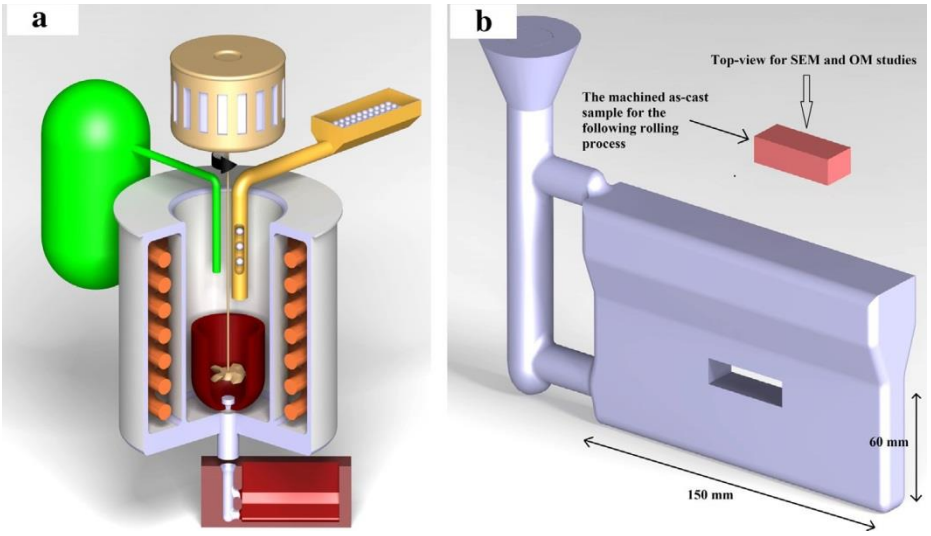

Fig. 3. Schematic of stir-casting set-up and the place that the samples were taken from the solidified composite for rolling and characterization.

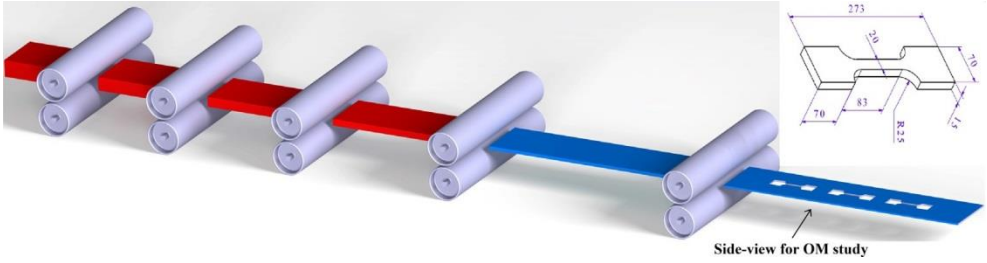

Fig. 4. Schematic of rolling process after casting and the dimension of tensile test samples.

3. Results and discussion

Figs. 5 and 6 show the morphology of copper coated Al_2O_3 (Fig. 5) and SiC (Fig. 6) particles after the ED process. As can be seen, most of the particles were coated by a copper layer. However, some uncoated parts could also be observed in Fig. 5, showing that the ED process for copper on large alumina particles can be difficult. Our previous study [19] indicated that the quality of copper coating on larger micron sized particles is not as good as on smaller particles. It was reported previously that the deposition time for smaller particles was higher than that for larger particles, indicating that finer particles have more time to be exposed to the deposition process [20]. Line EDAX analysis of Cu-coated alumina particles (see Fig. 5) shows the considerable presence of aluminum and oxygen on uncoated parts and the significant presence of copper on coated parts. Fig. 6 shows the morphology of copper-coated SiC particles with smaller average particle size. As can be seen, the particles were coated uniformly with suitable quality. No uncoated parts were detected during characterization of these powders.

As noted in Section 2, the coated ceramic particles were incorporated into semi-solid A356 at 600 C followed by stirring in the liquid-state. Fig. 7 shows the OM microstructures (500 magnification, top-view, see Fig. 3) of the A356 alloy and the composites after casting but before rolling. Fig. 7a shows the microstructure of as-cast A356 alloy (sample S_1) after 6 min stirring and solidification. The microstructure of semi-solid processed Al–Si alloys con sists of an aluminum region (with a-Al globular structure) and eutectic region (with Al/Si eutectic phases). The eutectic region contains Si, Mg_2Si as well as other possible embedded inter-metallic particles. Due to the eutectic reaction principles, the Si particles appear in the form of coarse sharp fibers [48].

Some round equiaxed a-Al grains were observed after solidifica tion, see Fig. 7a, showing that the semi-solid stirring lead to re-ordering of the dendritic structure. Clusters of acicular silicon phase were also observed at the grain-boundaries. It is important to note that a mixture of large a-Al globular grains as well as small equiaxed grains were formed after solidification when the slurry was poured into the mold from semi-solid state. Benefits of the implemented stir casting route in this work, where the metal was

poured from the liquid state, include that the mold was easily filled and that a uniform grainsize distribution was obtained.

Fig. 7b shows the microstructure of sample S_2 containing large alumina particles. As can be seen, the silicon phase formed at the vicinity of alumina particles. Fig. 7c presents the microstructure of sample S_3, in which fine SiC particles were incorporated into semi-solid alloy. In some cases, a cluster of particles was incorporated into the metal matrix, and in some cases, these particles were separated. In cases where particles were isolated, these small separated particles may have resulted from being pushed ahead of solidification front with final engulfment and incorporation with the matrix occurring before final solidification. Fig. 7d shows the microstructure of sample S_4, in which bimodal ceramic particles with bimodal particle size were incorporated into semi-solid melt of A356. Lower amounts of fine SiC were within clusters (noted by red[1]-colored circles) as well large alumina particles well integrated with the matrix were clearly observed. In order to evaluate the effect of particle type and size on the microstructure and grain size of the composites, Clemex software was used to measure grain size, results of which are given in Fig. 8.

From this results, it can be seen the fine SiC particles of sample S_3 did not affect the average grain size, when compared to the non-reinforced cast A356, while the larger alumina particles of sample S_3 did result in restricted grain growth. Sample S_4 had the lowest average grain size. This indicates that the finer reinforcement powders were also able to restrict the grain size if they were not clustered as in sample S_3. The simultaneous effects of large alumina particles and mostly separated SiC particles for sample S_4, therefore, resulted in the formation lower sized grains after solidification.

Optical micrographs of the side of the cast and rolled composites (see Fig. 4 for direction observation) are shown in Fig. 9. A highly altered composite microstructure was found in these composites. Fig. 9a shows sample S_1 without any ceramic particulate reinforcement. As can be seen, fragmented silicon phase was present within the eutectic, with higher sphericity compared to that present before rolling. The silicon and reinforcement phases were aligned with the rolling direction and presented a much more uniform distribution through the matrix. However even after the fivepasses of rolling, clustering of the SiC reinforcement could be observed in some parts. Fig. 9b and c shows that the microstructures of sample S_2 contain large alumina particles. The left image (Fig. 9b) shows the presence of the silicon phase with a better distribution around the alumina particles and their alignment along the rolling direction. This image also shows a fragmented fine alumina particle, which was separated during rolling from the larger particle. Fractured silicon particles around the alumina ceramic particle can be seen in this image. The right-hand image (Fig. 9c), with a higher magnification, shows two large alumina particles

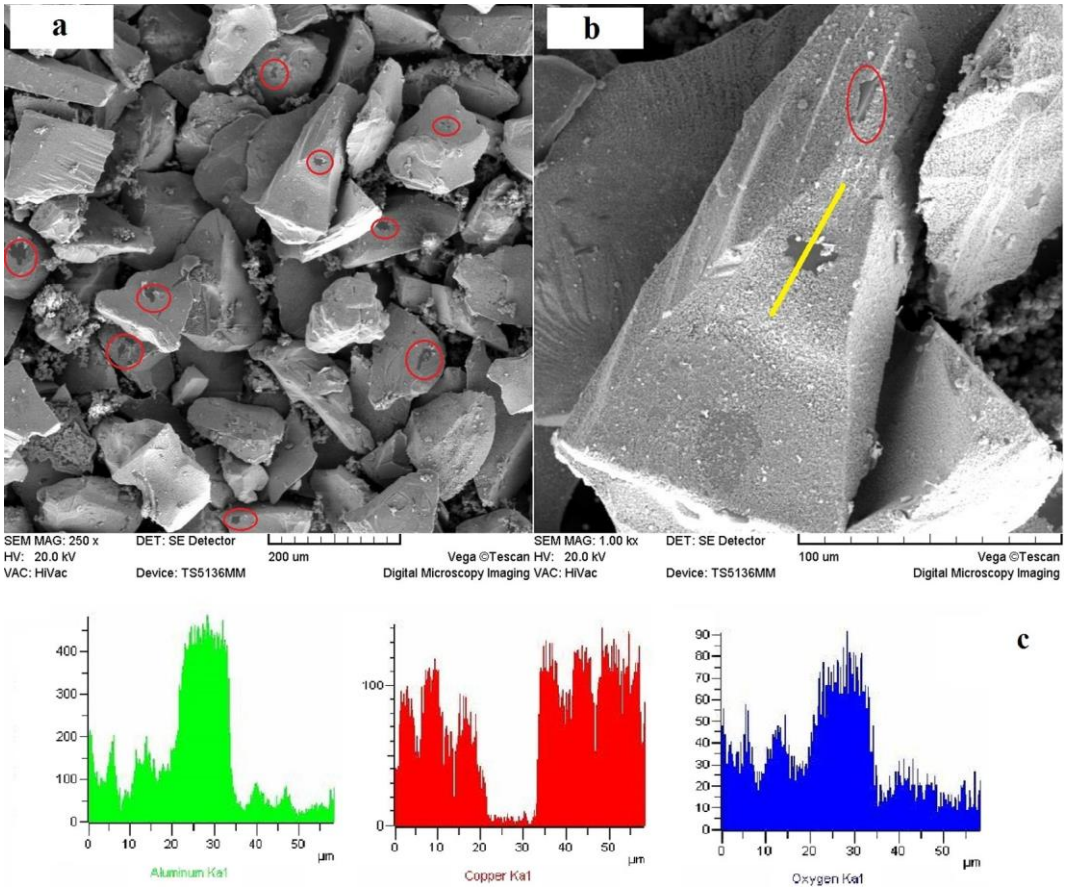

Fig. 5. Morphology of (a) copper coated Al_2O_3, (b) magnified view of uncoated region in (a), and (c) EDAX line scan results across coated and uncoated reion of (b).

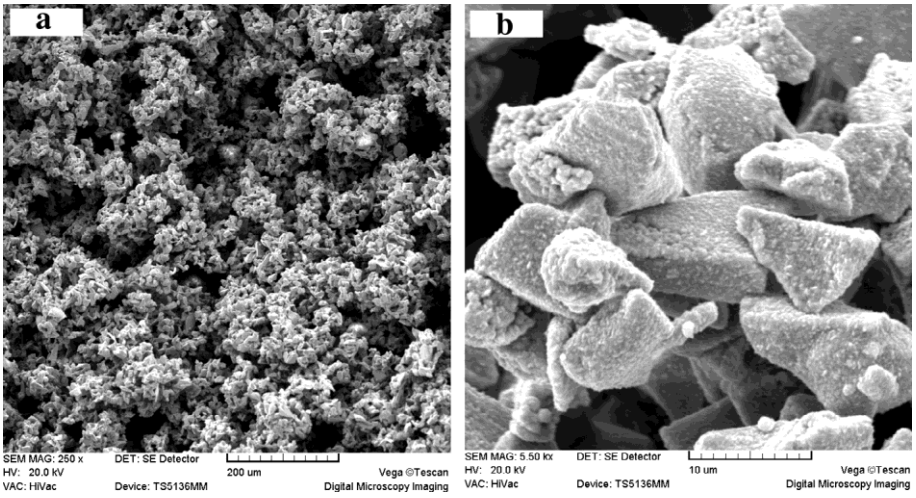

Fig. 6. Morphology of copper coated SiC particles.

which may have resulted from particle fracturing during the rolling process. Fig. 9d shows the OM microstructure of sample S_3. By comparing this microstructure with that of Fig. 7c, it can be observed that the rolling process was very effective at separating the fine agglomerated ceramic particles in this size range. These ceramic particles were aligned in a similar manner after rolling to the silicon particles, providing a more optimum uniform distribution in the matrix of A356 alloy. Fig. 9e and f shows the microstructure of sample S_4 that contains a bimodal distribution of ceramics particles. The distribution of fine SiC particles was observed to be better in sample S_4 than for sample S_3 (Fig. 9e), which might be partly due to the lower amount of SiC (1.5 wt.%) present. Pieces of the copper coating layer were detected in Fig. 9f, see orange-colored particles highlighted by rectangles. This indicates that the coating layer may have detached from the ceramic particles during the rolling process.

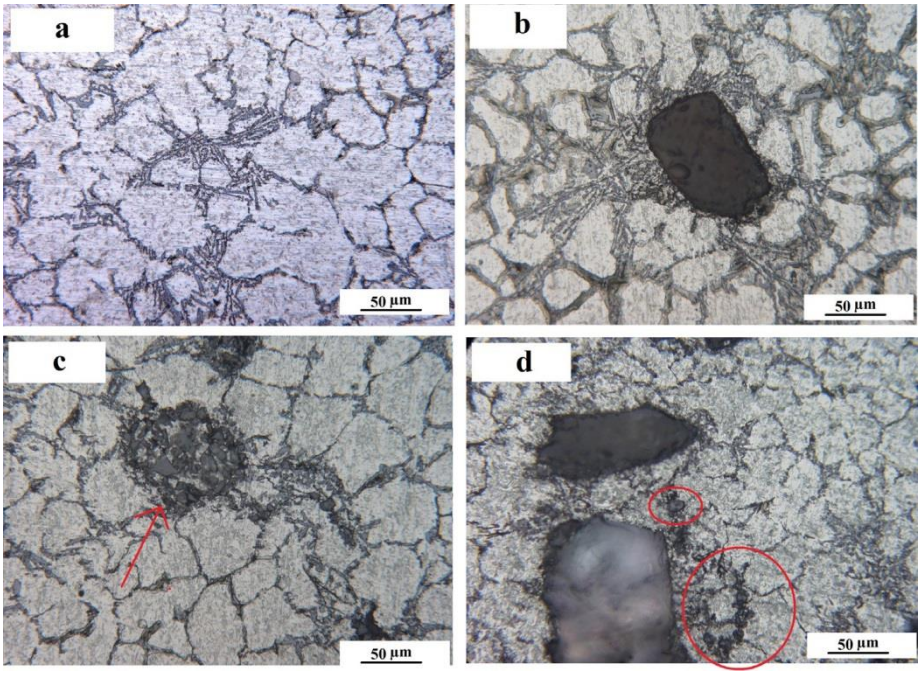

Fig. 7. OM microstructures (500 magnification, top-view) of samples S_1 (a), S_2, (b), S_3 (c), and S_4 (d).

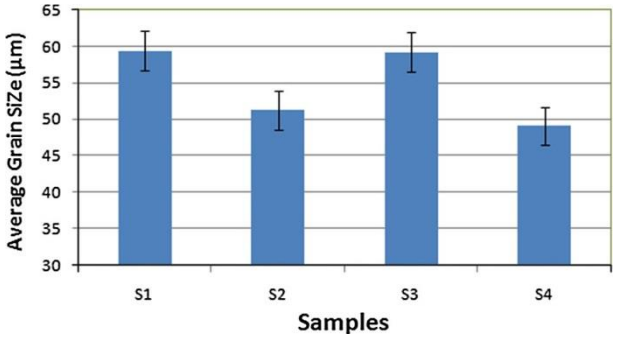

Fig. 8. The measured values of average grain size (lm) obtained using Clemex software from OM studies.

Fig. 10 shows SEM micrographs of the as-cast composites after 6 min stirring. Fig. 10a and b shows a low (left) and high (right) magnification SEM image of sample S_2. A considerable amount of ceramic particles were present in the low magnification SEM image with suitable distribution (left image), while some zones free of particle could be also observed. In addition, this sample also had considerable porosity. The right image (Fig. 10b) is a high-magnification backscattered electron (BSE) of sample S_2. This image shows an alumina particle that did not bond well with the matrix perhaps due to insufficient time or perhaps due to subsequent detachment due to the significant differences in thermal expansion coefficients between A356 and alumina. Point-EDAX analysis results showed that the whiter-colored parts in this image were rich in copper, indicating that the coating layer may have separated during the stirring process. Fig. 10c and d shows the micrograph of sample S_3 that contained the fine SiC reinforcement. Although particulate clustering was evident in this sample, this sample contained a reasonably uniform distribution of reinforcement as well as discrete locations of porosity. The white-colored parts observed in the right hand image of this sample were similar to those found in sample S_2, showing that the copper coating layer may be also be separating in this sample. In addition, porosity could be observed between the agglomerated fine particles where it would be difficult for liquid metal to feed during solidification. Fig. 10e and f shows the microstructures of sample S_4 that contained both the alumina and SiC ceramic particles. A reasonably uniform distribution of coarse and fine particles was observed in the low magnification SEM image (the left image) as well as the presence of porosities. The right image shows a small sized SiC particle with a good SiC-matrix interface and some remaining Cu coating.

Table 4 shows the relative density of the samples before and after the rolling process. As can be observed, the amount of porosities after casting process is considerable in particular for composite samples. The presence of these pores may have emanated from entrapped gasses during semi-solid stirring, solidification shrinkages, and the lack of ability for feed metal to flow between agglomerated ceramic particles. One of the requirements of using secondary mechanical processes after casting of AMMCs is the elimination of porosities and it can be found in Table 4 that rolling process significantly removed and eliminated the porosities of A356 alloy and its composites.

Table 5 shows the mechanical properties of the samples after the rolling process. A significant improvement about 48% in UTS, 59% in YS, 25% in hardness, and in particular 330% in ductility of the as-received ingot of A356 was obtained after semi-solid casting and rolling. However, the hardness value did not increase as much as the three other items. The fragmentation of dendrites and formation of equiaxed grains after semi-solid stirring, and fragmentation of silicon plates and distribution of silicon and reinforcement particles after the rolling process may have contributed to the considerable improvement in the mechanical properties between the as-cast A356 ingot and the sample S_1.

Table 4
Relative density of the samples as measured using the Archimedean method.

Samples	Relative density before rolling (%)	Relative density after rolling (%)
S_1	98.7	99.9
S_2	94.2	99.2
S_3	95.7	99.5
S_4	96.3	99.6

Table 5
Mechanical properties of the samples after the rolling process.

Sample	UTS (MPa)	Elongation (%)	YS (MPa)	Hardness (HV) at the	Hardness (HV) at the vicinity of ceramic
A356 (as-cast ingot)	146 ± 3	2.2 ± 0.1	93 ± 3	74 ± 2	–
Sample S_1	215 ± 3	9.5 ± 0.1	148 ± 3	92 ± 2	–
Sample S_2	254 ± 7	4.3 ± 0.5	183 ± 4	95 ± 2	167 ± 18
Sample S_3	266 ± 6	5.6 ± 0.3	191 ± 5	102 ± 3	170 ± 12
Sample S_4	302 ± 6	5.2 ± 0.2	237 ± 4	98 ± 6	190 ± 26

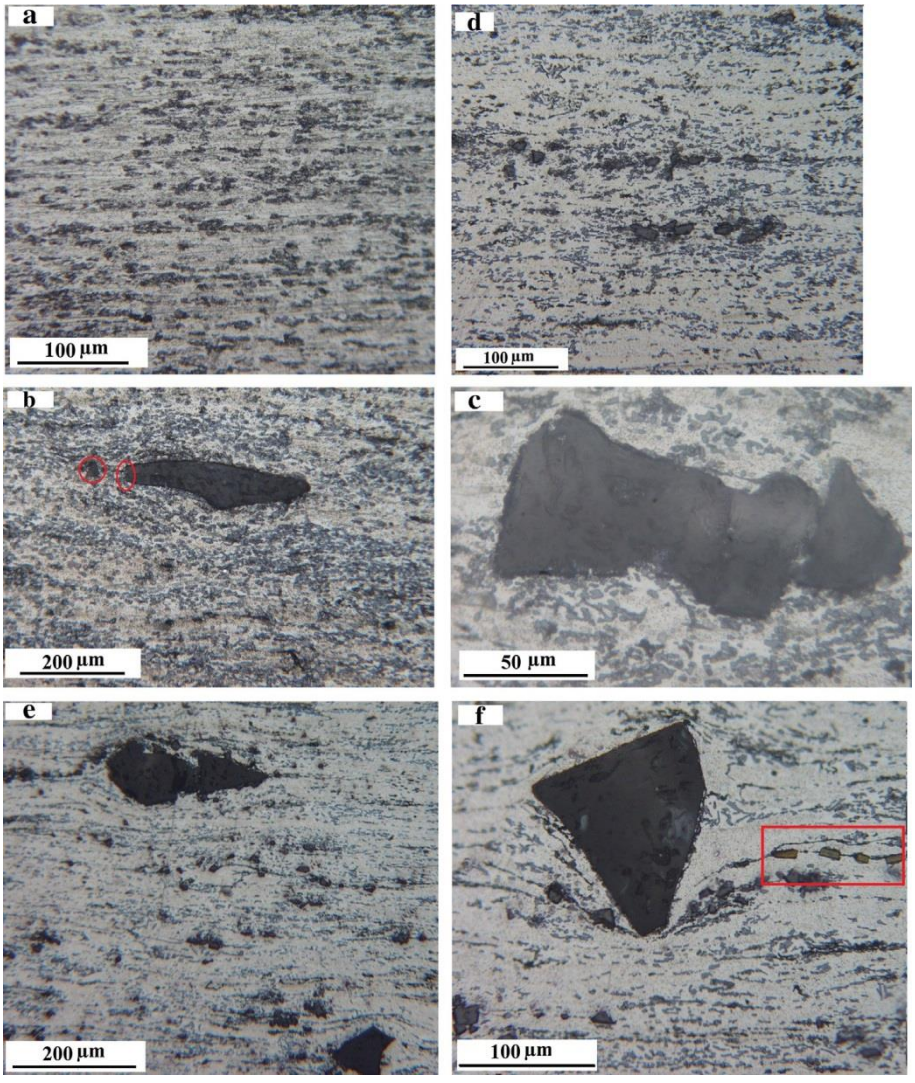

Fig. 9. Optical micrographs of rolled samples (a) S_1, (b and c) S_2, (d) S_3, and (e and f) S_4.

Table 5 shows that around a 20% increase in the UTS and YS occurred by addition of 3 wt.% Al_2O_3 to the sample (comparison between S_1 and S_2), while the ductility for the sample S_2 was about 50% lower than that of sample S_1. Although the larger alumina particles in sample S_2 produce a lower average grain size than sample S_3, higher strength, hardness, and ductility were obtained for the sample S_3 than sample S_2. In contrast with fine SiC particles, large Al_2O_3 particles are more prone to the fracturing during tensile test, providing a lower strength and ductility in S_2. The usage of finer ceramic particles with the same weight percent also lead to an increase in number of ceramic particles and reduced the zones free of particles. In addition, the quality of copper coating on the finer particles was better than on the coarser particles and its direct effect on improved incorporation of the ceramic particles are other strong reasons for the improved mechanical properties of sample S_3 above those obtained in sample S_2. Based on these four reasons, an increase of approximately 5% increase in UTS and YS does not present as sufficient reason for replacing the large alumina particles with the finer SiC powders. In fact, considerable agglomeration of the fine ceramic particles results in the sample S_3 not as stronger as may be expected. However, it should be noted that more than 30% increment was achieved for the ductility of the sample S_3 compared with than of the sample S_2. Excellent values of UTS, YS, ductility and hardness were obtained for the sample S_4 (about a 14% increase for UTS, 24% increase for YS, and a 12% increase for hardness compared with those of the sample S_3), which contained the bimodal ceramic particle distribution. The formation of a smaller grain size, a reduction in the agglomeration of fine SiC particles, lower fracturing and possible debonding of the large alumina particles due to their large size and incomplete coating layer, respectively, and a better distribution of ceramic particles in the matrix are four important reasons, which led to improved mechanical properties for the sample S_4.

Fig. 11a shows the fracture surface of sample S_1 that contained no ceramic particles. Small size dimples were observed on the fracture surface with no large facets, confirming the high ductility of this sample. Particle fracture of sample S_2 (see Fig. 11b, red-colored rectangles) was evident and this fracturing of the large alumina particles resulted in a composite with lower ductility as compared to the non-reinforced A356 stir casting and rolled sample S_1. Sample S_2 had the lowest ductility of all of the rolled samples, indicating that the larger particles were more prone for fracturing. However, Fig. 11b showing sample S_2, also shows the occurrence of

particle–matrix debonding at the interface (see red-colored circles) which would also contribute to the lowering the ductility of this sample. The strength of the metal/ceramic interface should also to some degree depend on the remaining of copper coating on the ceramic particles after stirring. Fig. 11c shows the fracture surfaces of sample S3. The presence of dimples and good bonding between a SiC particle and matrix (see the right image, red-colored rectangle) is evident in this figure. Fig. 11d shows the fracture surfaces of the sample S4, which had the highest strength and hardness results and relatively a similar ductility to the sample S3.

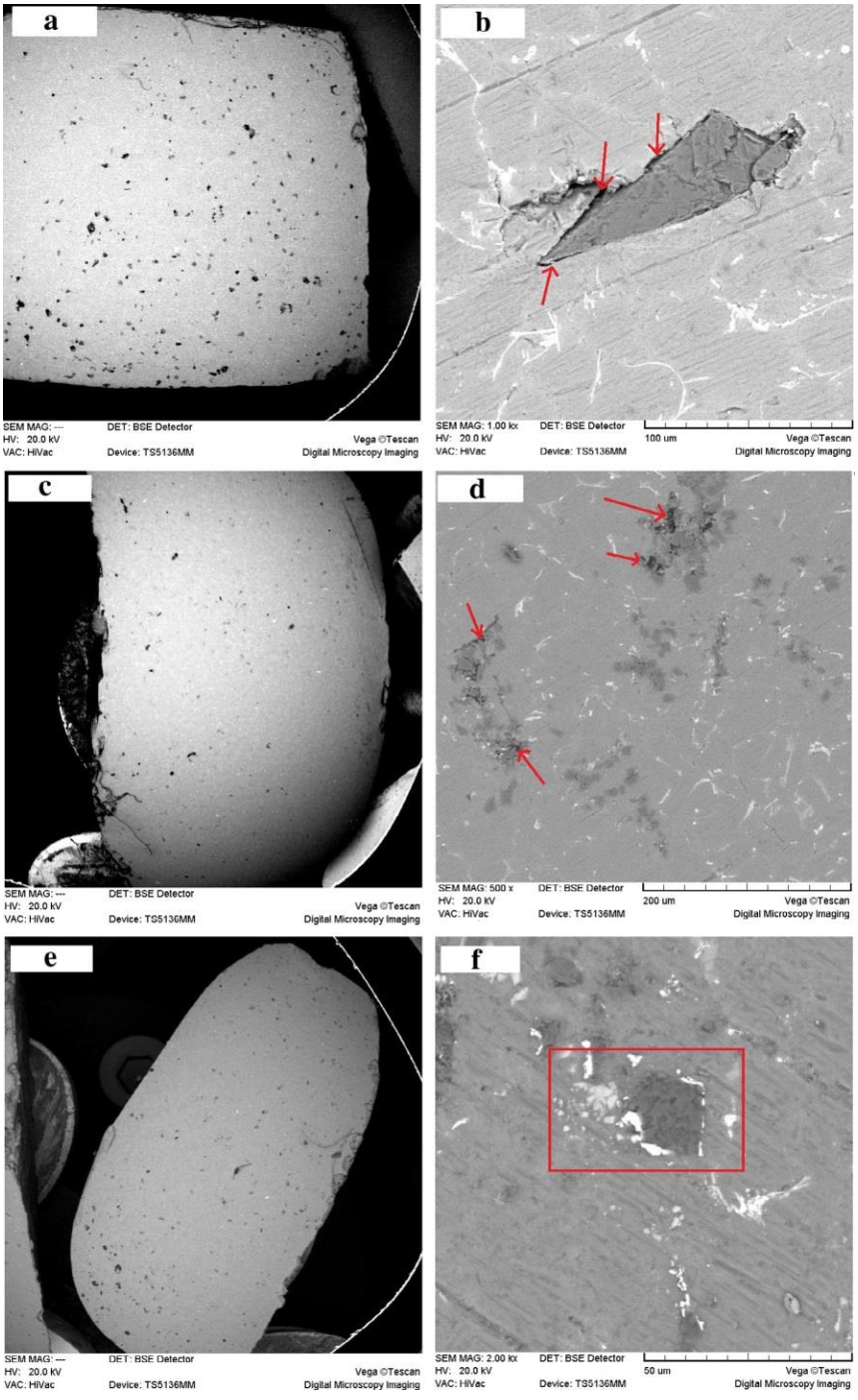

Fig. 10. Low and high magnification SEM images of the samples (a and b) S_2, (c and d) S_3, and (e and f).

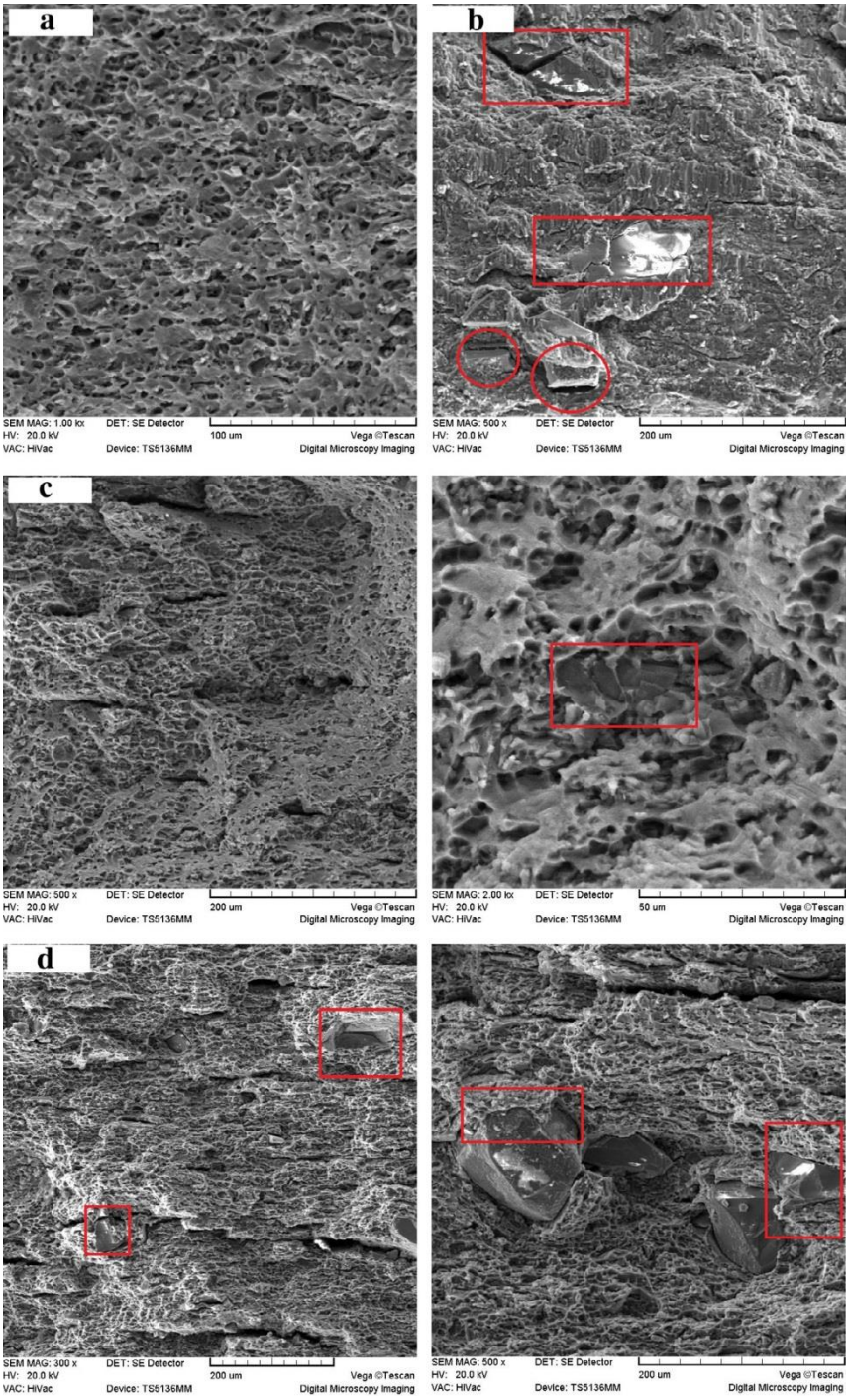

Fig. 11. SEM fracture surfaces of samples S_1 (a), S_2, (b), S_3 (c), and S_4 (d).

4. Conclusions

The effect of using a bimodal size distribution of two types of Cu-coated ceramic particle reinforcement with A356 matrix on microstructure and mechanical properties of the A356 based composites was investigated in this work. The effect of a two-step process, which consisted of semi-solid stir casting and rolling process was also studied. The results obtained are summarized below:

1. Copper electroless coating successfully covered the ceramic particles for their wettability improvement with molten aluminum alloy. However, it seems that due to a different between the deposition times of fine and coarse particles, various coating characteristics was obtained, in which the fine powders presented with a more uniform coating layer. A higher quality for

metal–ceramic interface was revealed after casting around Cu-coated SiC particles, in respect with Cu-coated Al_2O_3 particles, which considerably affected the fracture mechanism in the tensile test samples.

2. Ceramic particle agglomeration was revealed even by using copper coating and 1 wt.% Mg addition after casting and solidification for all the samples in particular for the samples contain fine SiC particles.
3. Large alumina particles provided a disruption to grain growth during composite solidification and resulted in small grain sizes.
4. The bimodal mixture of large alumina particles with small SiC particles resulted in the smallest average grain size between all of the samples. This is expected to be a result of the increased overall number of nucleation (local thermally initiated) sites for grain growth and perhaps restriction of grain growth due to enhanced distribution of the reinforcement particles.
5. A uniform distribution of silicon plates and SiC fine particles was obtained after the rolling process. In addition, an almost complete elimination of porosity was observed after this process.
6. It was revealed that copper coating layer was separated for some particles maybe during the stirring process. This has implications for choice of period of processing before casting as well as final bond strengths between the reinforcement and matrix.
7. A significant improvement in the mechanical properties were obtained for as-received ingot of A356 after semi-solid stir-casting and rolling. A UTS, YS, and hardness from the bimodal composite of 302 (MPa), 237 (MPa), and 144 (HV), respectively were established, which are considerably higher values than those obtained from the single distribution particle size produced composites, meaning that using a mixture of bimodal sized particles would be effective for the mechanical properties improvement in AMMCs. It was also found that Cu-coated SiC reinforced composite had a higher strength and in particular ductility in respect to Cu-coated Al_2O_3 particles reinforced composite.

References

[1] H. Ye, An overview of the development of Al–Si-alloy based material for engine applications, J. Mater. Eng. Perform. 12 (2003) 288–297.
[2] S. Prasad, R. Asthana, Aluminum metal–matrix composites for automotive applications: tribological considerations, Tribol. Lett. 17 (2004) 445–453.
[3] T. Srivatsan, T. Sudarshan, E. Lavernia, Processing of discontinuously- reinforced metal matrix composites by rapid solidification, Progr. Mater. Sci. 39 (1995) 317–409.
[4] S. Vijayarangan, N. Rajamanickam, V. Sivananth, Evaluation of metal matrix composite to replace spheroidal graphite iron for a critical component, steering knuckle, Mater. Des. 43 (2013) 532–541.
[5] M. Roshan, T.R. Mousavian, H. Ebrahimkhani, A. Mosleh, Fabrication of Al- based composites reinforced with Al_2O_3–Tib_2 ceramic composite particulates using vortex-casting method, J. Mining Metall., Sect. B: Metall.. 49 (2013) 299–305.
[6] N. Valibeygloo, R.A. Khosroshahi, R.T. Mousavian, Microstructural and mechanical properties of Al–4.5 wt% Cu reinforced with alumina nanoparticles by stir casting method, Int. J. Minerals Metall. Mater. 20 (2013) 978–985.
[7] M. Mohammadpour, R. Azari Khosroshahi, R. Taherzadeh Mousavian, D. Brabazon, Effect of interfacial-active elements addition on the incorporation of micron-sized SiC particles in molten pure aluminum, Ceram. Int. 40 (2014) 8323–8332.
[8] M. Mohammadpour, R.A. Khosroshahi, R.T. Mousavian, D. Brabazon, A novel method for incorporation of micron-sized SiC particles into molten pure aluminum utilizing a Co coating, Metall. Mater. Trans. B 46 (1) (2014) 12–19.
[9] J. Hashim, L. Looney, M. Hashmi, Metal matrix composites: production by the stir casting method, J. Mater. Process. Technol. 92 (1999) 1–7.
[10] S. Naher, D. Brabazon, L. Looney, Development and assessment of a new quick quench stir caster design for the production of metal matrix composites, J. Mater. Process. Technol. 166 (2005) 430–439.
[11] D. Brabazon, D. Browne, A. Carr, Mechanical stir casting of aluminium alloys from the mushy state: process, microstructure and mechanical properties, Mater. Sci. Eng.: A 326 (2002) 370–381.
[12] S. Tahamtan, A. Halvaee, M. Emamy, Z. Jiang, A.F. Boostani, Exploiting superior tensile properties of a novel network-structure AlA206 matrix composite by hybridizing micron-sized Al_3Ti with Al_2O_3 nano particulates, Mater. Sci. Eng.: A 619 (2014) 190–198.
[13] J. Hashim, L. Looney, M. Hashmi, The enhancement of wettability of SiC particles in cast aluminium matrix composites, J. Mater. Process. Technol. 119 (2001) 329–335.
[14] D. Kirkwood, Semisolid metal processing, Int. Mater. Rev. 39 (1994) 173–189. [15] O. Lashkari, R. Ghomashchi, The implication of rheology in semi-solid metal processes: an overview, J. Mater. Process. Technol. 182 (2007) 229–240.
[16] C. Quaak, M. Horsten, W. Kool, Rheological behaviour of partially solidified aluminium matrix composites, Mater. Sci. Eng.: A 183 (1994) 247–256.
[17] M. Paes, E. Zoqui, Semi-solid behavior of new Al–Si–Mg alloys for thixoforming, Mater. Sci. Eng.: A 406 (2005) 63–73.
[18] P. Seo, Kang, C. Kang, S. Lee, A study on reheating characteristics for thixo die casting process with electromagnetic stirring and extruded aluminum alloys and their mechanical properties, Int. J. Adv. Manuf. Technol. 43 (2009) 482–499.
[19] I. El-Mahallawi, Y. Shash, K. Eigenfeld, T. Mahmoud, R. Ragaie, A. Shash, et al., Influence of nanodispersions on strength–ductility properties of semisolid cast A356 Al alloy, Mater. Sci. Technol. 26 (2010) 1226–1231.
[20] N. Beigi Khosroshahi, R. Azari Khosroshahi, R. Taherzadeh Mousavian, D. Brabazon, Electroless deposition (ED) of copper coating on micron-sized SiC particles, Surf. Eng. 30 (2014) 747–751.
[21] A.F. Boostani, S. Tahamtan, Z. Jiang, D. Wei, S. Yazdani, R.A. Khosroshahi, et al., Enhanced tensile properties of aluminium matrix composites reinforced with graphene encapsulated SiC nanoparticles, Compos. Part A: Appl. Sci. Manuf. 68 (2015) 155–163.
[22] T. Rajan, R. Pillai, B. Pai, Reinforcement coatings and interfaces in aluminium metal matrix composites, J. Mater. Sci. 33 (1998) 3491–3503.
[23] W. Xue, Q. Jin, Q. Zhu, M. Hua, Y. Ma, Anti-corrosion microarc oxidation coatings on SiCP/AZ31 magnesium matrix composite, J. Alloys Comp. 482 (2009) 208–212.
[24] A. Urena, P. Rodrigo, J. Baldonedo, L. Gil, Active coatings for SiC particles to reduce the degradation by liquid aluminium during processing of aluminium matrix composites: study of interfacial reactions, J. Microscopy 201 (2001) 122–136.
[25] J. Rams, A. Ureña, M. Campo, Dual layer silica coatings of SiC particle reinforcements in aluminium matrix composites, Surf. Coat. Technol. 200 (2006) 4017–4026.
[26] A. Ureña, M. Escalera, L. Gil, Oxidation barriers on SiC particles for use in aluminium matrix composites manufactured by casting route: mechanisms of interfacial protection, Journal of materials science. 37 (2002) 4633–4643.
[27] P. Rohatgi, Cast aluminium alloy composites containing copper-coated ground mica particles, J. Mater. Sci. 16 (1981) 1599–1606.
[28] C. Leon, G. Mendoza-Suarez, R.A. Drew, Wettability and spreading kinetics of molten aluminum on copper-coated ceramics, J. Mater. Sci. 41 (2006) 5081–5087.
[29] S. Roy, B. Nataraj, S. Suwas, S. Kumar, K. Chattopadhyay, Accumulative roll bonding of aluminum alloys 2219/5086 laminates: microstructural evolution and tensile properties, Mater. Des. 36 (2012) 529–539.
[30] C. Xu, M. Furukawa, Z. Horita, T.G. Langdon, Influence of ECAP on precipitate distributions in a spray-cast aluminum alloy, Acta Mater. 53 (2005) 749–758.
[31] G. Ramu, R. Bauri, Effect of equal channel angular pressing (ECAP) on microstructure and properties of Al–SiCp composites, Mater. Des. 30 (2009) 3554–3559.
[32] D. Ma, J. Wang, K. Xu, Equal channel angular pressing of a SiC reinforced aluminum-based composite, Mater. Lett. 56 (2002) 999–1002.
[33] I. Sabirov, O. Kolednik, R. Valiev, R. Pippan, Equal channel angular pressing of metal matrix composites: effect on particle distribution and fracture toughness, Acta Mater. 53 (2005) 4919–4930.
[34] N. Haghdadi, A. Zarei-Hanzaki, H. Abedi, O. Sabokpa, The effect of thermomechanical parameters on the eutectic silicon characteristics in a non-modified cast

A356 aluminum alloy, Mater. Sci. Eng.: A 549 (2012) 93–99.

[35] F. Humphreys, W. Miller, M. Djazeb, Microstructural development during thermomechanical processing of particulate metal–matrix composites, Mater. Sci. Technol. 6 (1990) 1157–1166.
[36] Ü. Cöcen, K. Önel, Ductility and strength of extruded SiCp/aluminium-alloy composites, Compos. Sci. Technol. 62 (2002) 275–282.
[37] L. Ceschini, G. Minak, A. Morri, Forging of the AA2618/20 vol.% Al_2O_{3p} composite: effects on microstructure and tensile properties, Compos. Sci. Technol. 69 (2009) 1783–1789.
[38] M. Montoya-Dávila, M. Pech-Canul, M. Pech-Canul, Effect of bi-and trimodal size distribution on the superficial hardness of Al/SiC composites prepared by pressureless infiltration, Powder Technol. 176 (2007) 66–71.
[39] K. Chu, C. Jia, X. Liang, H. Chen, H. Guo, The thermal conductivity of pressure infiltrated SiCp/Al composites with various size distributions: experimental study and modeling, Mater. Des. 30 (2009) 3497–3503.
[40] R. Arpon, J. Molina, R. Saravanan, C. Garcia-Cordovilla, E. Louis, J. Narciso, Thermal expansion behaviour of aluminium/SiC composites with bimodal particle distributions, Acta Mater. 51 (2003) 3145–3156.
[41] J. Molina, J. Narciso, L. Weber, A. Mortensen, E. Louis, Thermal conductivity of Al–SiC composites with monomodal and bimodal particle size distribution, Mater. Sci. Eng.: A 480 (2008) 483–488.
[42] J. Molina, E. Piñero, J. Narciso, C. García-Cordovilla, E. Louis, Liquid metal infiltration into ceramic particle preforms with bimodal size distributions, Curr. Opin. Solid State Mater. Sci. 9 (2005) 202–210.
[43] H. Lee, S. Hong, Pressure infiltration casting process and thermophysical properties of high volume fraction SiCp/Al metal matrix composites, Mater. Sci. Technol. 19 (2003) 1057–1064.
[44] S. Kumar, R.S. Panwar, O. Pandey, Effect of dual reinforced ceramic particles on high temperature tribological properties of aluminum composites, Ceram. Int. 39 (2013) 6333–6342.
[45] M. Shen, X. Wang, C. Li, M. Zhang, X. Hu, M. Zheng, et al., Effect of bimodal size SiC particulates on microstructure and mechanical properties of AZ31B magnesium matrix composites, Mater. Des. 52 (2013) 1011–1017.
[46] K. Deng, J. Shi, C. Wang, X. Wang, Y. Wu, K. Nie, et al., Microstructure and strengthening mechanism of bimodal size particle reinforced magnesium matrix composite, Compos. Part A: Appl. Sci. Manuf. 43 (2012) 1280–1284.
[47] A.A. Cerit, Investigation of the low-speed impact behavior of dual particle size metal matrix composites, Mater. Des. 57 (2014) 330–335.
[48] R. Jamaati, S. Amirkhanlou, M.R. Toroghinejad, B. Niroumand, Significant improvement of semi-solid microstructure and mechanical properties of A356 alloy by ARB process, Mater. Sci. Eng.: A 528 (2011) 2495–2501.